South African Journal of Geomatics, Vol. 10. No. 2, August 2021

Comparative Evaluation and Analysis of Different Tropospheric Delay Models in Ghana

Samuel Osah, Akwasi Afrifa Acheampong, Isaac Dadzie, Collins Fosu

Department of Geomatic Engineering, College of Engineering, Kwame Nkrumah University of Science and Technology, Kumasi, Ghana

DOI: http://dx.doi.org/10.4314/sajg.v10i2.10

Abstract

Tropospheric delay prediction models have become increasingly important in Global Navigation Satellite System (GNSS) as they play a critical role in GNSS positioning applications. Due to the different atmospheric conditions over the earth regions, tropospheric effect on GNSS signals also differs, influencing the performance of these prediction models. Thus, the choice of a particular prediction model can significantly degrade the positioning accuracy especially when the model does not suit the user's environs. Therefore, a performance assessment of existing prediction models in various regions for a suitable one is very imperative. This paper evaluates and analyses seven commonly used tropospheric delay models in Ghana in terms of performances in Zenith Tropospheric Delay (ZTD) estimation and baseline positional accuracies using data from six selected Continuously Operating Reference Stations (CORS). The 1˚x1˚ gridded Vienna Mapping Functions 3 (VMF3) ZTD product and coordinates solutions from the CSRS-PPP positioning service were respectively used as references. The results show that the Black model performed better in estimating the ZTD, followed by Askne and Nordius model. The Saastamoinen, Marini and Murray, Niell, Goads and Goodman and Hopfield models respectively performed poorly. However, the result of the baseline solutions did not show much variation in the coordinate difference provided by the use of the prediction models, nonetheless, the Black and Askne and Nordius models continue to dominate the other models. Of all the models evaluated, either Black or Askne and Nordius model is recommended for use to mitigate the ZTD in the study area, however, the choice of the Black model will be more desirable.

Keywords: *GNSS, Tropospheric delay, Tropospheric delay prediction models, Vienna Mapping Functions 3 (VMF3), Multiple Comparison Test (MCT)*

1. Introduction

Global Navigation Satellite System (GNSS) is well noted for its 24-hour provision of all-weather precise three-dimensional (3D) Positioning, Navigation, Surveillance, and Timing capabilities on a global scale to all manner of users. Regardless of GNSS's enormous capabilities, the system is still faced with some major limitations and shortcomings that decrease the precision and accuracy of GNSS positioning. One of such limitations is the problem of delays in signal propagation through the Earth's atmospheric layers, primarily, the ionosphere and the troposphere. GNSS signals propagating

through the Earth's atmospheric layers, experience refraction due to the variations in refractivity along the signal transmission path, which changes the propagation speed and direction before arriving at the receiver. This results in time delay and bending and consequently causes an increase in the optical path lengths travelled by the signals more than the true geometric distances between the satellites in view and the receiver (Mendes, 1999; El-Rabbany, 2002). Thus, positioning accuracy is degraded by this phenomenon as range errors are introduced in the position solution.

Nonetheless, each atmospheric layer has a different impact on the GNSS signals, of which the ionospheric delay can to a large extent be removed by an ionosphere-free linear combination of dual or multi-frequency GNSS observables owing to its dispersive nature (Wang and Li, 2016). This leaves tropospheric delay as the major error source in GNSS applications (Ma *et al*., 2019). The impact of tropospheric delay ranges from about 2.0 to 2.6m in the zenith direction to about 20 to 28m near the horizon and at lower elevation angles (Sanlioglu and Zeybek, 2012). The extent of the impact of tropospheric delay on GNSS signals is further aggravated in the low-latitude or equatorial region due to the thicker tropospheric layer (up to 16km) and the hot conditions in this region (Musa *et al*., 2005). The thicker tropospheric layer exposes the low-latitude region to huge volumes and imbalance of water vapour content which significantly affects the propagating signals via the troposphere (Amir and Musa, 2011). However, Ghana's proximity to the equator makes Ghana more susceptible to the impact of the tropospheric delay. Tropospheric effects on GNSS signals, therefore, remain a major challenge and a growing concern to GNSS users particularly, in the low-latitude region (Musa *et al*., 2005). Modelling and/or mitigation is therefore required for precise GNSS positioning and navigational applications.

The most common technique used in mitigating tropospheric delay in GNSS applications is the use of empirical prediction models (Hu and Yao, 2019). A number of these prediction models have been developed and implemented in the various GNSS processing software for use to estimate and mitigate tropospheric delay error. The availability of these models provides users with countless means of selection in their applications to reduce the tropospheric effect on GNSS signals (Chen and Liu, 2016). However, since positioning accuracy is affected by the accuracy of the tropospheric delay model, an improperly selected tropospheric model may result in mismodelling of tropospheric delay which may significantly impair the performance of tropospheric delay mitigation, resulting in degrading the positioning accuracy up to an error of about 10m or more (Penna *et al*., 2001; Farah, 2020). But then again, the problem that arises is, which model best-suit the prevailing environs or atmosphere since the accuracies and performances of these prediction models differ under different atmospheric or climatic conditions (Opaluwa *et al*., 2013; Tuka and El-Mowafy, 2013). Consistent with Isioye *et al*. (2015) users in many instances employ a particular tropospheric model based on its popularity or those which are set as default in their processing software without giving adequate background as to why it should be used. Therefore, it is important to evaluate the impact and performance of these prediction models in different places or regions. This paper aims at evaluating and analysing seven commonly used tropospheric delay models in Ghana in terms of performances in estimating the ZTD and positional accuracies using one-month GNSS data from six selected

CORS. The 1˚x1˚gridded VMF3 ZTD product and coordinates solutions from the CSRS-PPP online positioning service were used as references and the optimal tropospheric model for the study area is recommended.

2. Tropospheric Delay Modelling

The troposphere forms the lower portion of the neutral atmosphere closest to the earth. It extends at a height of about 8 km over the poles and 16 km over the equator (Kos *et al*., 2009; Misra and Enge, 2011). The effect of the troposphere on GNSS signals is called tropospheric delay which induces an excess propagation path length on GNSS signals and emanates from the sum of the propagation delay and signal bending (Mendes, 1999). From Fermat's principle and following (Bevis *et al*., 1992; Mendes, 1999; Kleijer, 2004) the excess propagation path (ΔL_r^t) can be calculated by integration of the refractive index along the signal transmission path, s, from satellite, t to receiver, r at elevation angle (θ) via the troposphere as:

$$\Delta L_r^t(\theta) = S - G = \underbrace{\int_s \left(n(s)-1\right) ds}_{\textbf{Path delay}} + \underbrace{\left[\int_s ds - \int_G dG\right]}_{\textbf{Signal bending}} \quad [1]$$

$$S = \int_r^t c\,dt = \int_r^t \frac{c}{v} ds = \int_S n(s)\,ds \quad [2]$$

$$G = \int_{vacuum} dG = \int_G dG \quad [3]$$

where *S* is the optical or electromagnetic path length [m], c = speed of light in vacuum [ms-1], v= ds/dt, the propagation speed through the troposphere [ms-1], n=c/v, the refractive index, *G* is the geometric range along the straight path between *t* and *r* assuming the signal travel through a vacuum.

In the zenith direction (ZD) where satellites are directly overhead the receiver (i.e. θ = 90^o), the signal path is a straight line (i.e. *S* and *G* become identical) and the bending effect disappears with the assumption that the troposphere is horizontally stratified (Bevis *et al*., 1992; Mendes, 1999). Equation (1) now becomes:

$$\Delta L = \int_S \left[n(s)-1\right] ds \quad [4]$$

Expressing *n* in terms of total refractivity *N*, where $N = 10^{-6}\left(n-1\right)$, equation (4) can be rewritten as:

$$\Delta L = 10^{-6} \int_s N(s)\,ds \quad [5]$$

N is a function of meteorological parameters such as pressure [*P*(*mbar*)], temperature [(*T* (*K*)] and relative humidity [*RH* (*%*)] or water vapour partial pressure [*e* (*mbar*)] along the signal transmission

path and can be separated into hydrostatic or dry (N_d) and wet (N_w) components caused by dry gases (mainly N_2, O_2) and water vapour respectively (Sanz *et al.*, 2013).

$$N = N_d + N_w \quad [6]$$

The refractivity (N) can be related to the meteorological parameters (P, T, e) as as (Smith and Weintraub, 1953):

$$N = \underbrace{\left[k_1 \frac{P}{T}\right]}_{N_d} + \underbrace{\left[k_2 \frac{e}{T} + k_3 \frac{e}{T^2}\right]}_{N_w} \quad [7]$$

k_1, k_2, k_3 are refractivity constants whose values according to Bevis *et al* (1994) are given as $k_1 = 77.60 \pm 0.05\ K/hpa$, $k_2 = 70.40 \pm 2.2\ K/hpa$, $k_3 = 373900 \pm 1200\ K^2/hpa$.

Re-writing equation (5)

$$\Delta L = 10^{-6} \int_S [N_d + N_w] ds = 10^{-6} \int_S N_d(s) ds + 10^{-6} \int_S N_w(s) ds \quad [8]$$

Expressing equation (8) in terms of ZTD,

$$ZTD = 10^{-6} \int_{ZD} N_d(s) ds + 10^{-6} \int_{ZD} N_w(s) ds \quad [9]$$

Equation (9) can further be written as:

$$ZTD = \underbrace{10^{-6} \int_h^{TOA} N_d(h) dh}_{ZHD} + \underbrace{10^{-6} \int_h^{TOA} N_w(h) dh}_{ZWD} \quad [10]$$

where, h is the height of station or receiver antenna, and TOA is the top of the atmosphere. It can be seen from equation (8-10) that, ZTD is the sum of the Zenith Hydrostatic Delay (ZHD) and the Zenith Wet Delay (ZWD) expressed as

$$ZTD = ZHD + ZWD \quad [11]$$

With an appropriate mapping function and using the satellite elevation angle(θ) as input, the ZTD can be resolved into the Slant Tropospheric Delay (STD) as:

$$STD = ZHD \times MF_h(\theta) + ZWD \times MF_w(\theta) \quad [12]$$

$$STD = SHD + SWD \quad [13]$$

where MFh and MFw represent the hydrostatic and wet mapping functions respectively, SHD and SWD are the slant hydrostatic and wet tropospheric delays respectively.

The ZHD accounts for about 90% of the ZTD and can easily be modelled or predicted to sub-millimetre accuracy by empirical prediction models using surface meteorological observations; whereas the ZWD accounts for the remaining 10% of the ZTD. In contrast to the ZHD, the ZWD

cannot be precisely modelled or predicted due to its large spatial and temporal variability (Younes, 2016; Zhang *et al*., 2016). The troposphere is characterized as being a non-dispersive medium for radio frequencies up to 15 GHz, hence its effect is independent of GNSS frequencies and therefore affects carrier phase and code measurements equally (Sanz *et al*., 2013).

2.1. Tropospheric Delay Models

Tropospheric delay models are categorized into two (Sun *et al.*, 2019). ***The first category,*** the traditional models, require real-time surface meteorological observations at the user's environs to predict the tropospheric delays at decimeter to centimetre level of accuracy. ***The second category***, the blind models, is not dependent on observed meteorological parameters but require user location and time information for the prediction of tropospheric delay computed from climatological data or forecast of Numeric Weather Prediction (NWP) models. This paper compares the performances of the first category (traditional models). The following sub-sections give a brief description of the various traditional tropospheric models used in this study.

2.1.1. Refined Saastamoinen Model (SAAS)

The general form of the Refined Saastamoinen model with mapping function for the computation of STD is written as:

$$STD = \frac{0.002277}{\cos z}\left[P + \left(\frac{1255}{T} + 0.05 \right) e - \beta \tan^2 z \right] + \delta R \qquad [14]$$

where P is the pressure in hPa, e is the partial pressure of water vapour in hPa, T is the temperature in Kelvin, z is the zenith angle, β and δR are correction terms dependent on the height of the station and the zenith angle given in a tabular form. Details of table can be inferred from (Hofmann-Wellenhof *et al.*, 2008) and (Xu and Xu, 2016).

2.1.2. Hopfield Model (HOP)

By using two-quartic refractivity profiles expressed as a function of height of the 4th degree above the Earth surface, Hopfield (1969) developed the SHD and SWD models given as (Hofmann-Wellenhof *et al.*, 2008):

$$SHD = \frac{10^{-6}}{5} 77.64 \frac{P}{T}\left[40136 + 148.72\left(T - 273.16 \right) \right] \cdot \frac{1}{\sin\sqrt{\theta^2 + 6.25}} \qquad [15]$$

$$SWD = \frac{10^{-6}}{5} \times \left(-12.96T + 3.718 \times 10^5 \right) \frac{e}{T^2} \times 11000 \cdot \frac{1}{\sin\sqrt{\theta^2 + 2.25}} \qquad [16]$$

2.1.3. Goad and Goodman Model (GG)

Goad and Goodman model (Goad and Goodman, 1974), also known as the modified Hopfield model stems from the modification of Hopfield model by the use of lengths of position vectors instead of heights (Hofmann-Wellenhof *et al.*, 2008). The STD by Goad and Goodman can be summarized as (Goad and Goodman, 1974; Hofmann-Wellenhof *et al.*, 2008; Xu and Xu, 2016):

$$STD = \Delta_d^{Trop}\left(E\right) + \Delta_w^{Trop}\left(E\right) \quad [17]$$

where

$$\Delta_i^{Trop}\left(E\right) = 10^{-6} N_i \left[\sum_{k=1}^{9}\left(\frac{\alpha_{i,k}}{k}\right) r_i^k\right] \quad [18]$$

$\alpha_{1,i} = 1$; $\alpha_{2,i} = 4a_i$; $\alpha_{3,i} = 6a_i^2 + 4b_i$ $\alpha_{4,i} = 4a_i\left(a_i^2 + 3b_i\right)$; $\alpha_{5,i} = a_i^4 + 12a_i^2 b_i + 6b_i^2$
$\alpha_{6,i} = 4a_i b_i\left(a_i^2 + 3b_i\right); \alpha_{7,i} = b_i^2\left(6a_i^2 + 4b_i\right)$ $\alpha_{8,i} = 4a_i b_i^3$; $\alpha_{9,i} = b_i^4$

$$a_i = -\frac{\sin E}{h_i} \qquad b_i = -\frac{\cos^2 E}{2h_i R_E} \quad [19]$$

$$r_i = \sqrt{\left(R_E + h_i\right)^2 - R_E^2 \cos^2 E - R_E \sin E} \quad [20]$$

the subscript i is used to identify the dry and wet components of the tropospheric delay (i.e. $i = d, w$), N is the refractivity, r is the range to the top of the dry or wet component, h_i is the topmost point where the wet or dry component becomes zero, E is the satellite elevation angle.

N_d and N_w can be expressed as (Xu and Xu, 2016):

$$N_d = 77.64\left(\frac{P}{T}\right),\ N_w = -12.96\left(\frac{e}{T}\right) + 371800\left(\frac{e}{T^2}\right) \quad [21]$$

2.1.4. Black Model

By utilizing Hopfield model, (Black, 1978) proposed a simple analytical form in the integration of the refractivity. The hydrostatic and wet components of the model are as follows:

$$SHD = 2.343P.\left[\frac{\left(T - 4.12\right)}{T}\right].I\left(h = h_d, E\right) \quad [22]$$

$$SWD = K_w.I\left(h = h_w, E\right) \quad [23]$$

where

$I(h = h_d, E)$ is the mapping function given as (Black, 1978):

$$I(h,E) = \left[1 - \left(\frac{\cos E}{1 + (1 - l_C) \cdot \frac{h}{r_s}}\right)^2\right]^{-\frac{1}{2}} \quad [24]$$

At higher elevations (i.e. E >30˚), Black (1978) proposed

$I(h,E) = \cos ecE$, $l_C = 0.167 - (0.076 + 0.00015(T - 273.15))\exp^{-0.3E}$

$h_d = 148.98(T - 4.12)$ in [meters] above the station, $h_w = 13{,}000$ in [meters]

E is the Satellite elevation angle in [degrees], r_s is the distance from the centre of the earth to the station in [meters]. For elevation angles of 5˚ and above, a choice of $l_C = 0.85$ gives an error no greater than 4.5 cm.

Considering the difficulty in modelling the wet component of the tropospheric delay, (Black, 1978) suggested the following regional empirical constants:

K_w = 0.28 m for summer in tropic or mid-latitude regions, 0.20 m for spring or fall in mid-latitudes, 0.12 m for winter in maritime mid-latitudes, 0.06 m for winter in continental mid-latitudes, and 0.05 m for polar regions.

2.1.5. Askne and Nordius Model (AN)

Askne and Nordius model (Askne and Nordius, 1987) for the computation of tropospheric path delay is based on a two-parameter closed-form model of atmospheric profile analysis. The ZHD and ZWD are given as (Askne and Nordius, 1987):

$$ZHD = 10^{-6} \frac{k_1 R_d}{g_m} P \quad [25]$$

$$ZWD = 10^{-6} \left(k_2' + k_3 / T_m\right) \frac{R_d}{(\lambda + 1) g_m} e \quad [26]$$

where T_m is the weighted mean temperature(K) given as:

$$T_m = T\left(1 - \frac{\alpha R_d}{(\lambda + 1) g_m}\right) \quad [27]$$

$k_2' = k_2 - k_1 \frac{M_w}{M_d} = 16.52 Kmbar^{-1}$, $k_1 = 77.604 \pm 0.014$, K/mbar

$k_2 = 64.79 \pm 0.08$ K/mbar , $k_3 = 373900 \pm 0.004$ K^2 / mbar

M_w and M_d are the molar mass of water (18.0152 g/mol) and dry air (28.9644 g/mol) respectively, R_d is the molar gas constant (8.314 $Jmol^{-1}K^{-1}$), λ and α are the water vapour and temperature lapse rates respectively. g_m is the gravity acceleration at the mass centre of a vertical column of the atmosphere above the GNSS receiver antenna computed as:

$$g_m = 9.784(1 - 0.00266\cos 2\varphi - 2.8\times10^{-7} H) \quad [28]$$

The Askne and Nordius model provides only zenith delays and has no internal mapping function. We employed the Black and Eisner mapping function model (Black and Eisner, 1984) for the computation of the slant delays which can be expressed as (Black & Eisner, 1984):

$$m(E) = \left[1 - \left(\frac{\cos E}{1 + 0.001}\right)^2\right]^{-1/2} \quad [29]$$

2.1.6. Marini and Murray Model (MM)

Marini and Murray Model (Marini and Murray Jr, 1973) model was based on the modification of Saastamoinen model using a continued fraction form. The total delay in the slant direction can be expressed as (Marini & Murray, 1973):

$$STD = \frac{1}{f(\phi, H)} \times \frac{A + B}{\sin E + \dfrac{B}{(A + B)(\sin E + 0.015)}} \quad [30]$$

$$A = 0.00235 \times P + 0.000141 \times e \quad [31]$$

$$B = \left(1.084\times10^{-8}\right) P \cdot T \cdot K + \left(4.734\times10^{-8}\right)\frac{P^2}{T} \cdot \frac{2}{3 - 1/K} \quad [32]$$

$$K = 1.163 - 0.00968\cos 2\phi - 0.00104T + 0.00001435P \quad [33]$$

$$f(\phi, H) = 1 - 0.0026\cos 2\phi - 0.00031H \quad [34]$$

e can be computed from a relative humidity measurement Rh (%) as (Marini & Murray,1973):

$$e = \frac{Rh}{100} \times 6.11 \times 10^{\frac{7.5(T - 273.15)}{237.3 + (T - 273.15)}} \quad [35]$$

2.1.7. Niell Model

Niell model is the blend of Saastamoinen zenith delays and the Niell mapping function (Niell, 1996) model (Dodo *et al.*, 2019). The Niell Mapping Function (NMF) formulation is a function of station latitude and observation time and it is based on the interpolation of the average and seasonal amplitude values given in a tabular form at 15˚ latitudinal interval. The general form of the model for both hydrostatic and wet mapping functions can be expressed as:

$$m(\varepsilon) = \frac{1+\dfrac{a}{1+\dfrac{b}{1+c}}}{\sin(\varepsilon)+\dfrac{a}{\sin(\varepsilon)+\dfrac{b}{\sin(\varepsilon)+c}}} \quad [36]$$

However, the addition of height correction term to the hydrostatic term differentiates the two models. Thus, the final hydrostatic mapping function mf_h is given as:

$$mf_h = m(\varepsilon) + H_s 10^{-3} M_h \quad [37]$$

$$M_h = \frac{1}{\sin(\varepsilon)} \frac{1+\dfrac{a_{ht}}{1+\dfrac{b_{ht}}{1+c_{ht}}}}{\sin(\varepsilon)+\dfrac{a_{ht}}{\sin(\varepsilon)+\dfrac{b_{ht}}{\sin(\varepsilon)+c_{ht}}}} \quad [38]$$

H_s is the height of the station, ε is the elevation angle, a, b, and c are empirical coefficients with different values for the hydrostatic and wet terms. a_{ht}, b_{ht}, c_{ht} are the coefficients in the height component. a, b, and c can be computed as follows

$$a(\varphi, t) = a_{avg}(\varphi) + a_{amp}(\varphi)\cos\left(2\pi(doy - 28)/365.25\right) \quad [39]$$

where φ is the station latitude, *doy* is the day of year, a_{avg}, a_{amp} are the average and seasonal amplitude values which can be obtained by the linear interpolation between the nearest latitudes. The similar procedure is applicable to b and c.

3. Materials and Methods

3.1. Data Acquisition

Data acquired in this study include GNSS data from GNSS CORS in Ghana, Meteorological parameters derived from the GPT3 model, and ZTD data obtained from the gridded VMF3-ZTD products. The following sub-sections summarize the various datasets used in this study.

3.1.1. GNSS Data

One month of GNSS data spanning from September 1 to September 30, 2019, were collected from six GNSS CORS located in four regions of Ghana, namely, Bolgatanga (Upper East region), Kumasi (Ashanti region), Accra (Greater Accra region), Takoradi and Tarkwa (Western region). Details of the stations and their locations in WGS 84 are shown in Table 1 and Figure 1.

3.1.2. Meteorological Data

None of the CORS used in this study is equipped with ground-based meteorological sensors for the provision of in-situ meteorological parameters. However, in the absence of in-situ surface meteorological observations, the empirical blind tropospheric delay models can be used for the provision of accurate surface meteorological parameters (Böhm *et al.*, 2015). This study utilized the recent blind tropospheric delay model, Global Pressure and Temperature 3, GPT3 (Landskron and Böhm, 2018). GPT3 is a refinement of the GPT2w (Böhm *et al.*, 2015) model. GPT3 provides the mean values plus annual and semi-annual amplitudes of various surface meteorological parameters such as pressure[$P(hpa)$], temperature [$T\,(^{\circ}C)$] and its lapse rate [$dT(^{\circ}C/km)$], water vapour pressure [$e(hpa)$] and its decrease factor [λ(dimensionless)], weighted mean temperature [$Tm(K)$]. These parameters are based on the analysis of monthly mean pressure level profiles of the European Centre for Medium-Range Weather Forecasts (ECMWF) ERA-Interim reanalysis for a period of 10 years (2001-2010). The model is provided on a regular 1° x 1° and 5° x 5° global grids. Each meteorological parameter can be computed using the equation below:

$$r(t) = A_0 + A_1 \cos\left(\frac{doy}{365.25}2\pi\right) + B_1 \sin\left(\frac{doy}{365.25}2\pi\right) + A_2 \cos\left(\frac{doy}{365.25}4\pi\right) + B_2 \sin\left(\frac{doy}{365.25}4\pi\right) \quad [40]$$

where A_0 is the mean value, (A_1, B_1) and (A_2, B_2) are the annual and semi-annual amplitudes of the selected parameters r, doy is the day of the year. Meteorological parameters retrieved in this study are P, T, e, Tm and λ on the 1° x 1° grid.

3.1.3. VMF ZTD Data

The Vienna Mapping Functions (VMF) formally the Global Geodetic Observing System (GGOS) atmosphere provides global gridded VMF1 and VMF3 zenith tropospheric products (http://vmf.geo.tuwien.ac.at/trop_products/GRID). They are generated from the ECMWF reanalysis data and are provided every 6 hours daily at four epochs 00, 06, 12 and 18 UTC. VMF3 is the successor of VMF1 realized on both 1˚ and 5˚ global grids (Landskron and Böhm, 2018). This study utilized the 1˚ gridded VMF3-ZTD products as a reference for evaluating the prediction models ZTD following (Yao *et al.*, 2016; Sun *et al.*, 2017) and also owing to the fact that the CORS employed in this study are not International GNSS Service (IGS). The precision and accuracy of the VMF-ZTD data have been investigated and validated against the IGS-ZTDs by (Yao *et al.*, 2017, 2018) to be accurate enough for tropospheric delay mitigation, model development and validation.

3.2. Data Processing

(i) ***GNSS data processing*** - 24 hours GNSS data in rinex format collected from the six selected CORS were processed at 60-seconds sampling rate and 10˚ elevation cut-off using goGPS software version 0.5.2 beta 1(Realini and Reguzzoni, 2013; Herrera *et al*., 2016). The relative positioning technique on both code and carrier-phase double-difference was utilized with Kalman filtering using the LISAG_SPINTEX station as the base and the remaining stations as rovers. A total of five baselines, shown in table 2, were processed. Two processing strategies were employed:

Strategy I: processing without the application of tropospheric delay model.

Strategy II: processing with the application of the tropospheric delay models.

(ii) ***Extraction of VMF3-ZTD*** – To obtain the VMF3-ZTD at the various CORS, we needed to interpolate the VMF3-ZTD to the exact location and time of each COR station. So, the stations' ellipsoidal coordinates (latitude, longitude, and height) and modified Julian (mjd) date obtained from the rinex observation data were used. The extraction was done using the MATLAB coded script or m-file '*SearchReadVMFgrids.m*', which is a modified version of the file *vmf3_grid.m* written by Landskron and Böhm (2018). The *vmf3_grid.m* file can be obtained at http:// vmf.geo.tuwien.ac.at/codes/ (last access 23 September 23, 2020). For each epoch grid file (e.g. 00 UT), a spatial interpolation to the specified locations of the CORS is first performed using the four surrounding grid points that are closest to the specified locations. A bilinear interpolation is then employed to interpolate the zenith delays at the grid points heights. By employing formulae suggested by Kouba (2008), the zenith delays at the grid heights are then transferred to the respective height of the COR stations using the orography file, *orography_ell_1x1*. Finally, the zenith delays (ZHD and ZWD) at the current epoch are obtained by a linear interpolation using values from two surrounding epochs. The average daily ZTD is obtained by adding the average daily ZHD and ZWD values.

It is worth mentioning that the prediction models used in this study and other ancillary information relating to tropospheric delay modelling were all coded and implemented in the goGPS v0.5.2 beta 1 software. The processed station coordinates in Universal Transverse Mercator (UTM) from the two processing strategies as well as the estimated ZTD from strategy II were extracted for analysis.

Table 1: GNSS stations in Ghana selected for this study.

Station	Code	City	Region	Latitude	Longitude	Height (m)
CREF0001	CREF	Bolgatanga	Upper East	10°47'48.84"	-0°51'25.55"	242.690
LISAG_ADUM	LSA_A	Kumasi	Ashanti	6° 41' 16.61"	-1°37'30.81"	308.396
LISAG_SPINTEX	LSA_S	Accra	Greater Accra	5° 38' 1.27"	-0° 5' 15.54"	75.583
SGGA C2600	SGGA	Accra	Greater Accra	5° 40' 25.67"	-0°10'29.15"	87.761
LISAG_TAKORADI	LSA_TAD	Takoradi	Western	4° 55' 31.75"	-1°46'26.63"	43.661
LISAG_TARKWA	LSA_TAR	Tarkwa	Western	5° 17' 51.72"	-2° 0' 0.15"	108.333

Table 2: Processed Baselines of the various CORS

Baseline	Length(km)	ΔH(m)
LSA_S - CREF	580.33	167.107
LSA_S - SGGA	10.62	12.177
LSA_S - LSA_A	206.49	232.813
LSA_S - LSA_TAD	202.65	-31.923
LSA_S - LSA_TAR	214.95	32.749

Figure 1: Map of Ghana showing the Regions of GNSS COR.

4. Results and Discussion

In order to investigate the performance of the prediction models, SAAS, HOP, GG, Black, Niell, AN and MM in the study area, the estimated ZTD obtained from each of the prediction models was compared with the interpolated gridded VMF3-ZTD dataset. Likewise, the final station UTM coordinate solutions [North(N), East(E), Height(h)] from the two processing strategies were also compared to their corresponding reference coordinates obtained from the CSRS-PPP online positioning service. The statistical quantities, mean Bias and Root Mean Square Error (RMSE) of each model ZTD and coordinate solution were computed for each station using equation (48) and a summary of the results are presented in Table 3 and Figure 2, 3, 5, 6, 7, 8, 9 and 10.

$$\begin{cases} Bias = \dfrac{1}{n}\sum_{i=1}^{n}\left(v_i^{MR} - v_i\right) \\ RMSE = \sqrt{\dfrac{1}{n}\sum_{i=1}^{n}\left(v_i^{MR} - v_i\right)^2} \end{cases} \quad [41]$$

where n is the number of observations, v_i^M and v_i^R are the estimated ZTD and UTM coordinates by the models and reference respectively.

To further investigate the performances of these models, a multiple comparison test (MCT) with 'scheffe' method (McHugh, 2011; Lee and Lee, 2018) was carried out to find out if the performances of the seven tropospheric delay models in relation to their RMSE values are significantly different from one another at 5% significant level using Matlab multicompare function. The MCT is used to determine which pairs of means are significantly different, and which pairs are not. The 'scheffe' method allows all possible comparisons/contrasts, both simple and complex to determine which tests are significant. The Null and Alternate hypothesis (H0, Ha) tests are stated as follows:

H0: The difference between the means is equal to 0.

Ha: The difference between the means is different from 0.

The result of the MCT is shown in Figure 4. Figure 4 provides an interactive graph with each group mean represented by a symbol and a comparison interval or bar represented by a line extending out from the symbol. Two groups (models) means are significantly different if their intervals are disjoint and they are not significantly different if their intervals overlap or intersect. For a selected group, the comparison bar is highlighted blue and all other groups that are significantly different are highlighted red. The bars for the groups that are not significantly different are grey as shown in Figure 4.

Table 3: Statistical Results of ZTD Bias/RMSE for each Model using VMF3 Data (unit: cm).

Model	Bias	RMS	Bias	RMS	Bias	RMS	Bias	RMS	Bias	RMS
	CREF		SGGA		LSA_A		LSA_TAD		LSA_TAR	
AN	1.87	2.35	3.09	3.53	1.81	2.32	1.32	1.8	2.17	2.61
BLACK	2.48	2.83	0.92	2.43	1.69	2.19	0.46	1.31	2.12	2.6
GG	8.14	8.27	6.75	7.02	7.6	7.74	7.17	7.3	7.81	7.95
HOP	8.76	8.88	7.53	7.78	8.18	8.31	7.68	7.8	8.44	8.57
MM	7.47	7.61	6.06	6.37	6.93	7.08	6.52	6.67	7.17	7.33
NEILL	7.54	7.68	6.18	6.48	6.99	7.14	6.57	6.72	7.21	7.36
SAAS	7.46	7.6	6.11	6.42	6.9	7.06	6.51	6.65	7.14	7.29

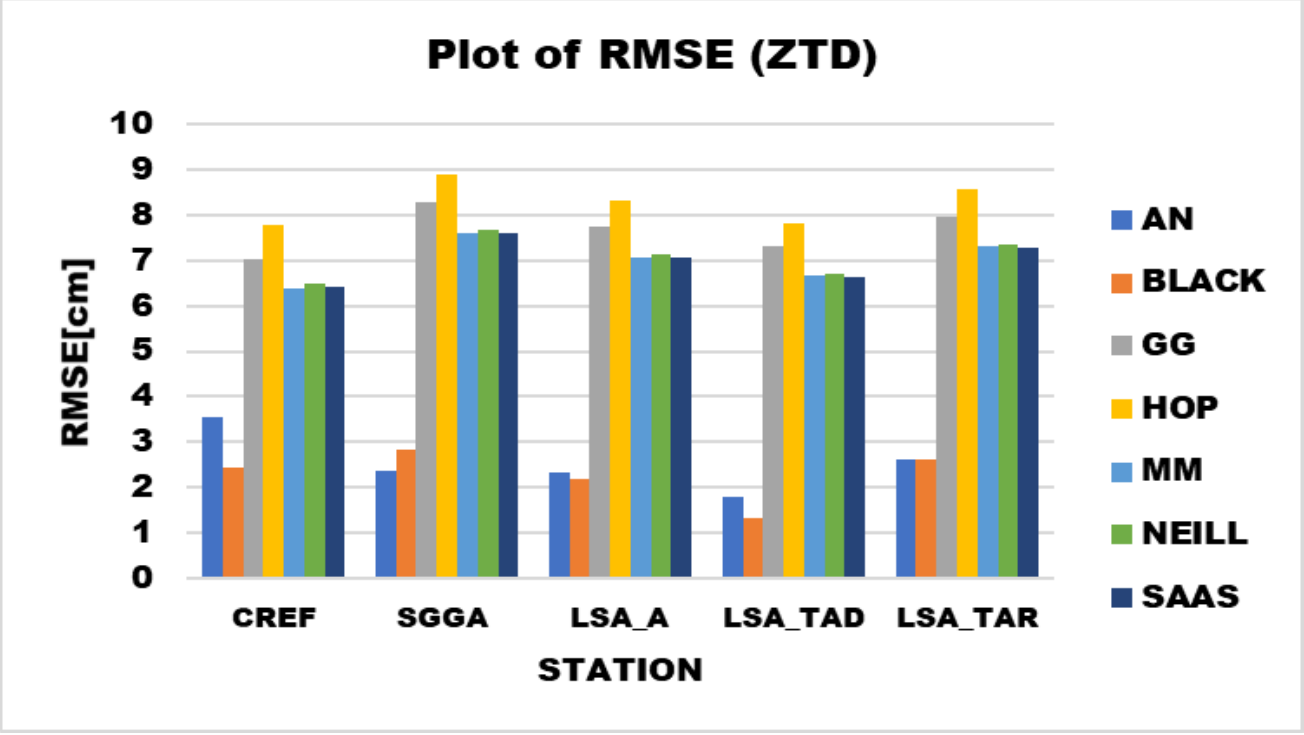

Figure 2: Comparison of RMSE of models ZTD at stations.

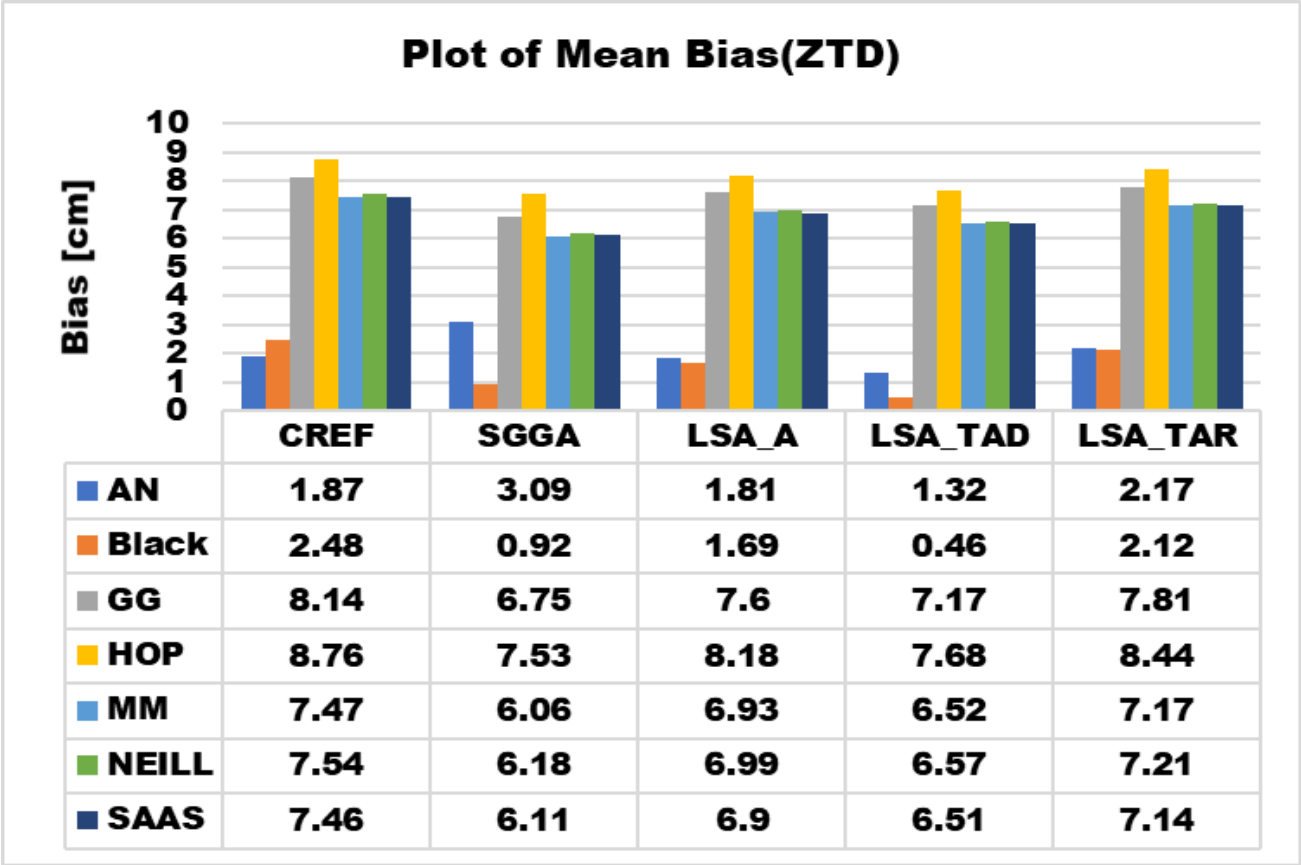

	CREF	SGGA	LSA_A	LSA_TAD	LSA_TAR
AN	1.87	3.09	1.81	1.32	2.17
Black	2.48	0.92	1.69	0.46	2.12
GG	8.14	6.75	7.6	7.17	7.81
HOP	8.76	7.53	8.18	7.68	8.44
MM	7.47	6.06	6.93	6.52	7.17
NEILL	7.54	6.18	6.99	6.57	7.21
SAAS	7.46	6.11	6.9	6.51	7.14

Figure 3: Comparison of models ZTD bias at stations.

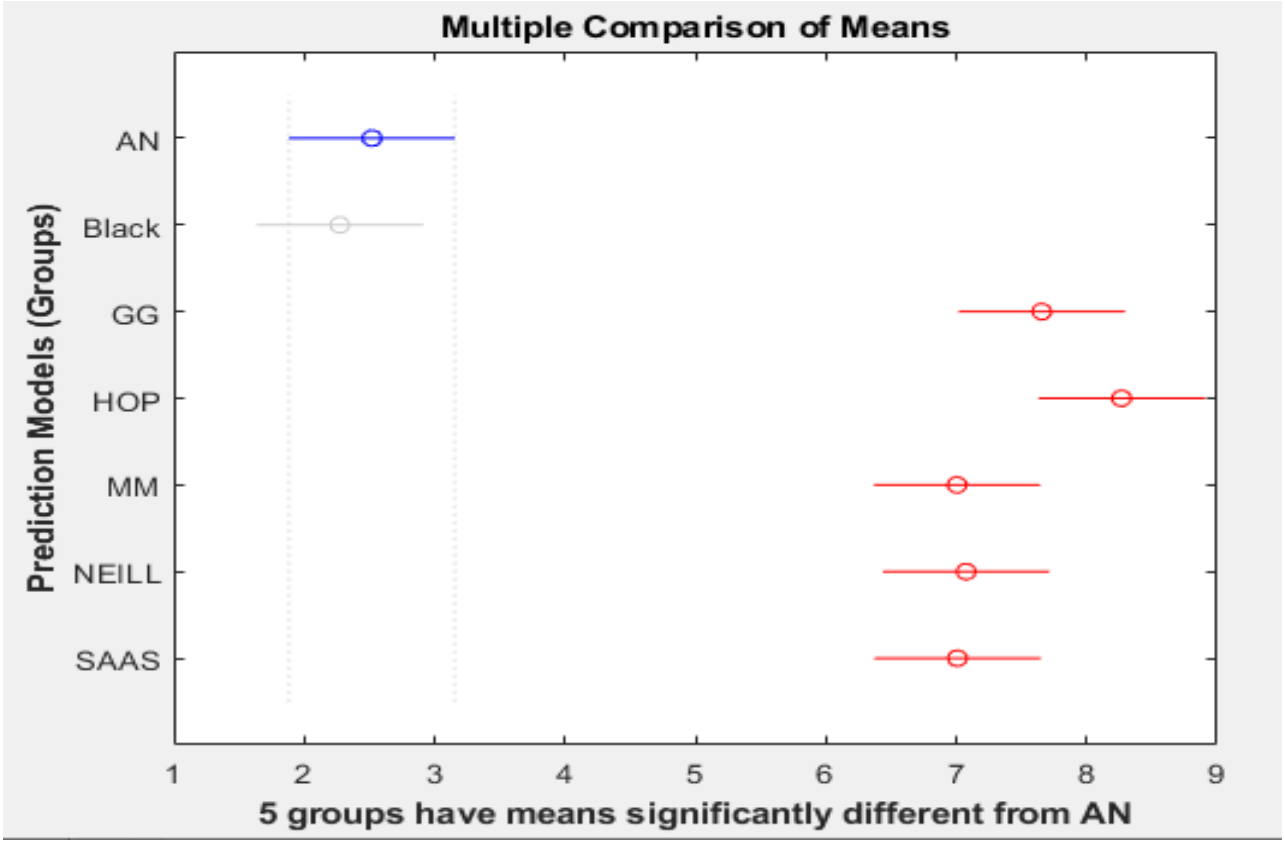

Figure 4: Multiple Comparison of Group (Models) Means.

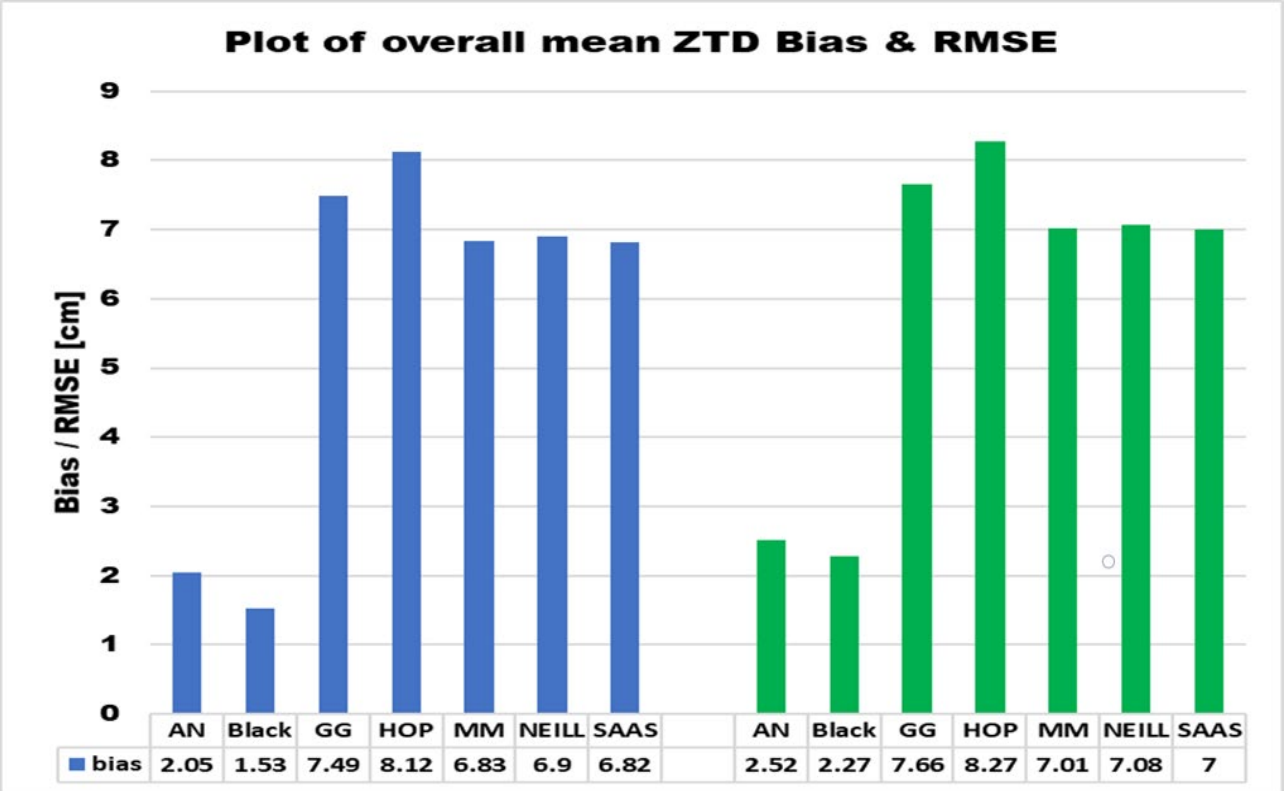

Figure 5: Comparison of mean Bias (left) and RMSE (right) of models ZTD.

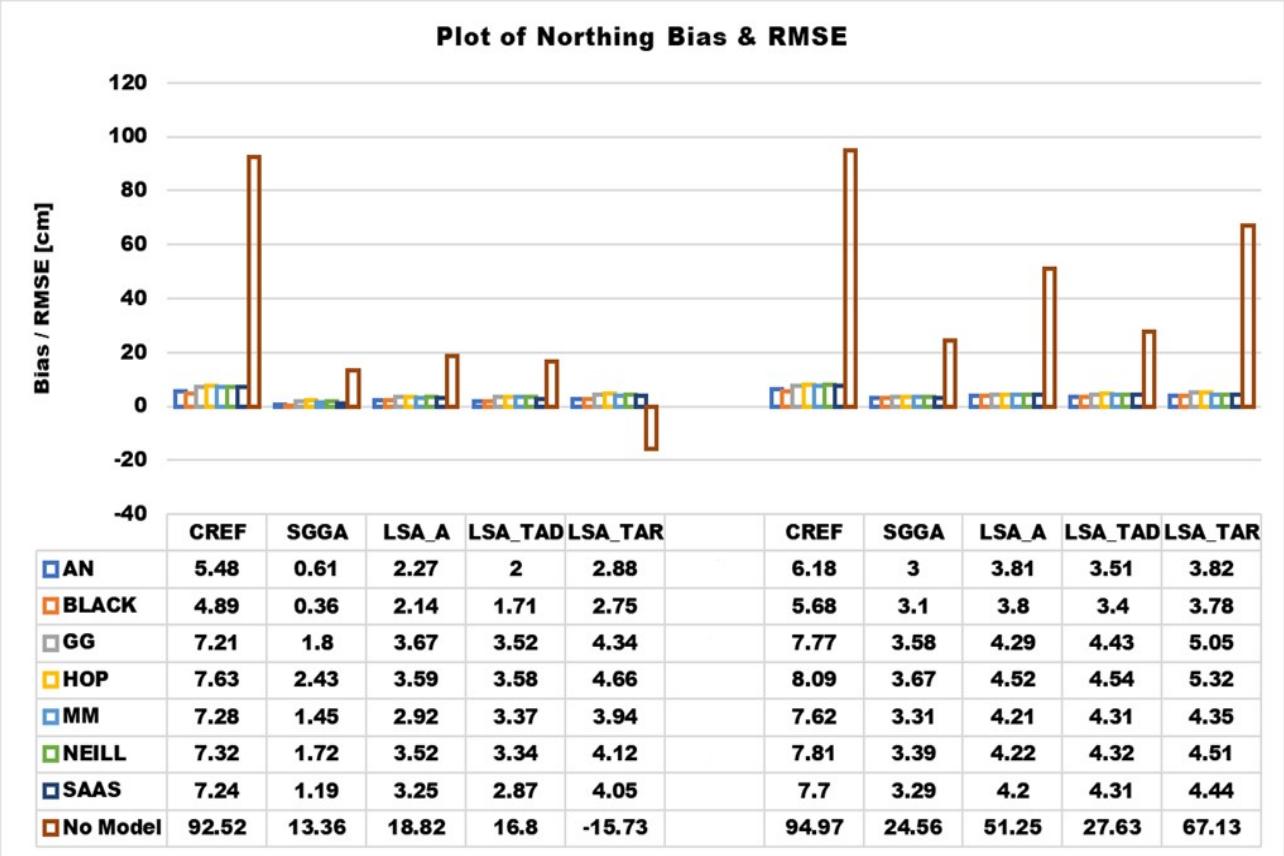

	CREF	SGGA	LSA_A	LSA_TAD	LSA_TAR	CREF	SGGA	LSA_A	LSA_TAD	LSA_TAR
AN	5.48	0.61	2.27	2	2.88	6.18	3	3.81	3.51	3.82
BLACK	4.89	0.36	2.14	1.71	2.75	5.68	3.1	3.8	3.4	3.78
GG	7.21	1.8	3.67	3.52	4.34	7.77	3.58	4.29	4.43	5.05
HOP	7.63	2.43	3.59	3.58	4.66	8.09	3.67	4.52	4.54	5.32
MM	7.28	1.45	2.92	3.37	3.94	7.62	3.31	4.21	4.31	4.35
NEILL	7.32	1.72	3.52	3.34	4.12	7.81	3.39	4.22	4.32	4.51
SAAS	7.24	1.19	3.25	2.87	4.05	7.7	3.29	4.2	4.31	4.44
No Model	92.52	13.36	18.82	16.8	-15.73	94.97	24.56	51.25	27.63	67.13

Figure 6: Comparison of Bias (left) and RMSE (right) of models Northing UTM coordinates.

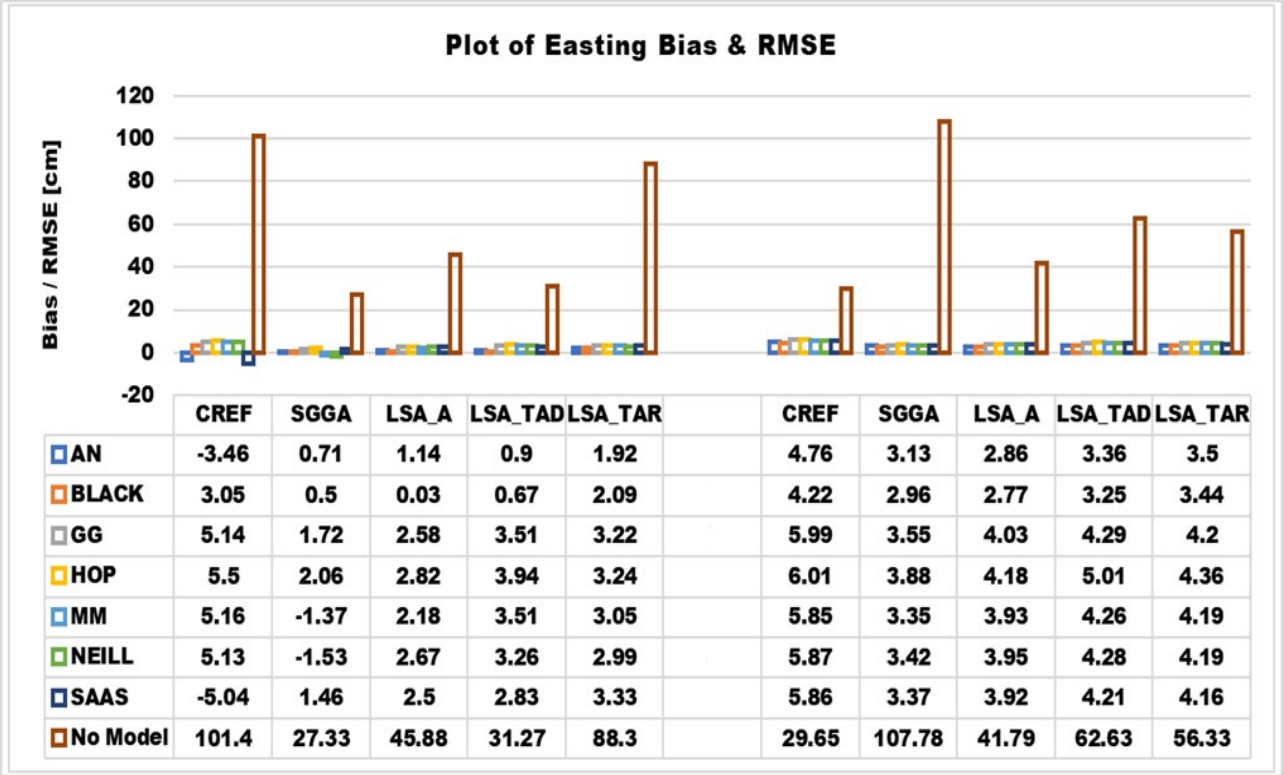

	CREF	SGGA	LSA_A	LSA_TAD	LSA_TAR	CREF	SGGA	LSA_A	LSA_TAD	LSA_TAR
AN	-3.46	0.71	1.14	0.9	1.92	4.76	3.13	2.86	3.36	3.5
BLACK	3.05	0.5	0.03	0.67	2.09	4.22	2.96	2.77	3.25	3.44
GG	5.14	1.72	2.58	3.51	3.22	5.99	3.55	4.03	4.29	4.2
HOP	5.5	2.06	2.82	3.94	3.24	6.01	3.88	4.18	5.01	4.36
MM	5.16	-1.37	2.18	3.51	3.05	5.85	3.35	3.93	4.26	4.19
NEILL	5.13	-1.53	2.67	3.26	2.99	5.87	3.42	3.95	4.28	4.19
SAAS	-5.04	1.46	2.5	2.83	3.33	5.86	3.37	3.92	4.21	4.16
No Model	101.4	27.33	45.88	31.27	88.3	29.65	107.78	41.79	62.63	56.33

Figure 7: Comparison of Bias (left) and RMSE (right) of models Easting UTM coordinates.

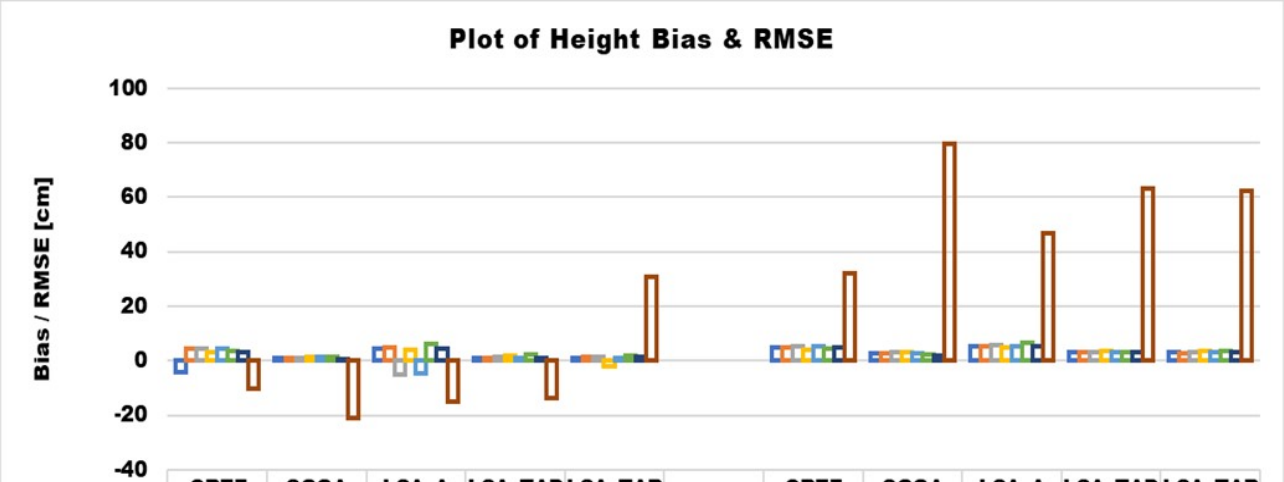

	CREF	SGGA	LSA_A	LSA_TAD	LSA_TAR	CREF	SGGA	LSA_A	LSA_TAD	LSA_TAR
AN	-4.12	0.83	4.57	1.16	1.05	4.97	2.78	5.31	3.16	2.93
BLACK	4.26	0.87	4.64	0.96	1.32	4.99	2.78	5.24	3.12	2.81
GG	4.46	0.78	-4.91	1.4	1.29	5.18	2.96	5.79	3.06	3
HOP	3.12	1.48	3.8	1.78	-2.23	4.12	3.24	4.7	3.37	3.51
MM	4.54	1.42	-4.61	0.81	0.99	5.37	2.7	5.48	3.08	3.1
NEILL	3.37	1.39	6	2.08	1.7	4.41	2.06	6.48	3.06	3.44
SAAS	3.16	0.56	4.46	1.1	1.59	4.7	1.98	5.26	2.97	3
No Model	-10.39	-21.18	-15.17	-13.6	30.89	32.14	79.62	46.67	63.29	62.37

Figure 8: Comparison of Bias (left) and RMSE (right) of models Heights.

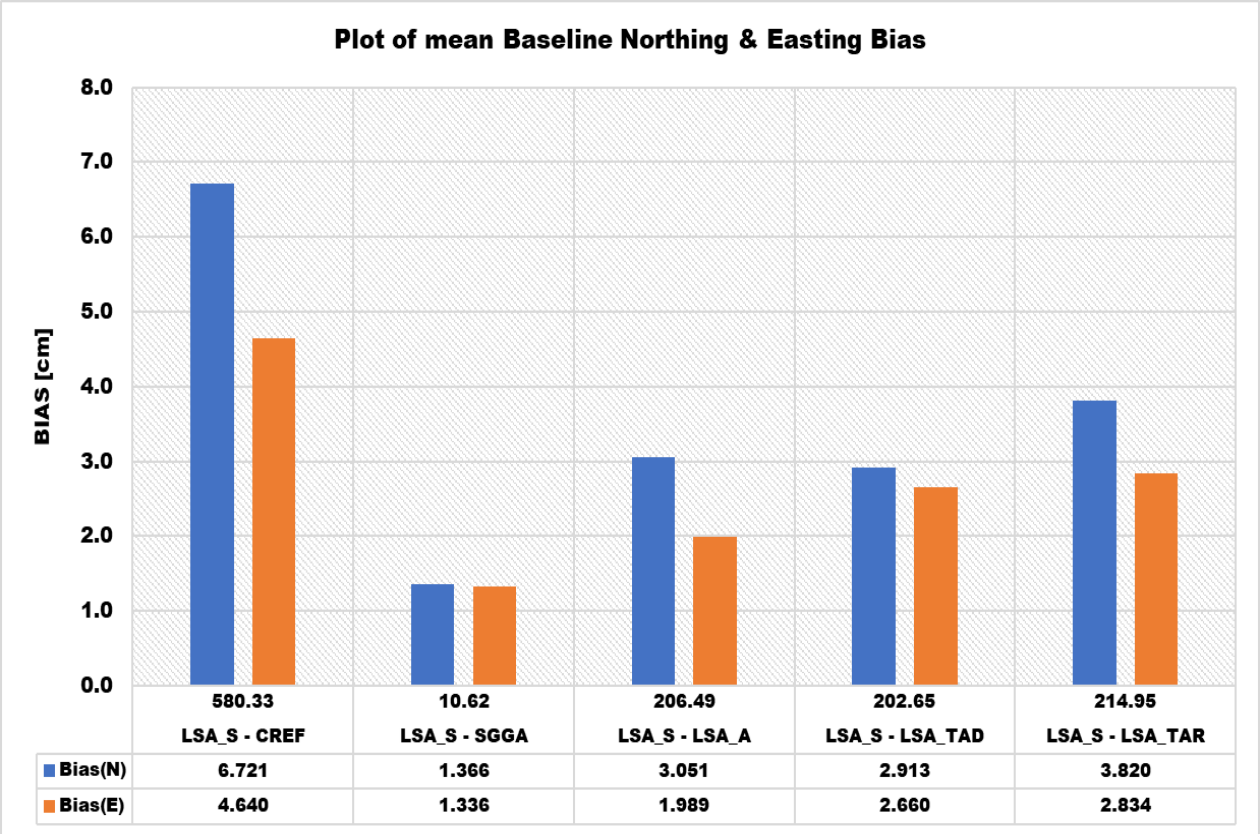

Figure 9: Comparison of mean Baseline Northing and Easting Bias.

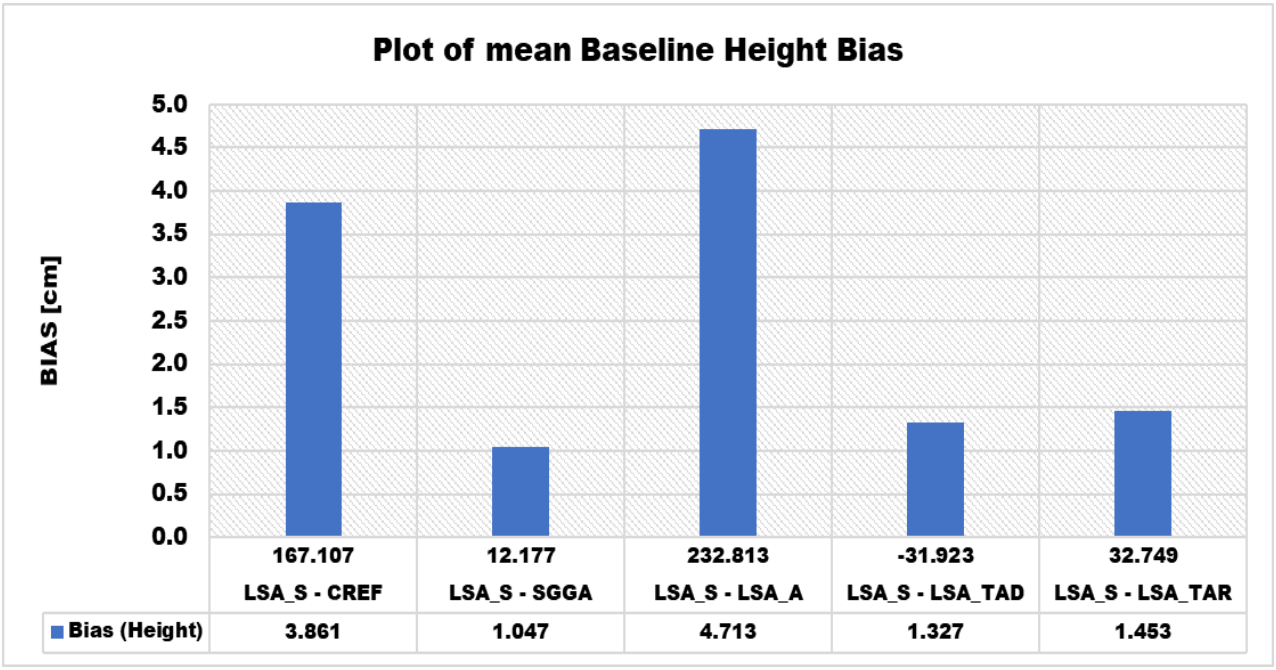

Figure 10: Comparison of mean Baseline Height difference (Bias).

4.1. Models Assessment Based on estimated ZTD

The performances of the prediction models are evaluated by comparing their estimated ZTDs with those derived from the gridded VMF3 ZTD data. From the results in Table 3 and Figure 2, 3 and 5 it can be seen that the mean ZTD bias and RMSE for the black and Askne and Nordius models are very small compared to Saastamoinen, Marini and Murray, Niell, Goads and Goodman, and Hopfield models which gave large bias and RMS errors respectively. The smaller the bias and RMS errors, the better the model's predictions.

The difference in performance is mainly due to the modelling of the wet component of the tropospheric delay in the models particularly the assumption made about the distribution of water vapour within the troposphere (Hofmann-Wellenhof *et al.*, 2008; Li *et al.*, 2008). For instance, the Black model assumes regional empirical constants that vary according to season and climate. Though Black model assumes constant wet delays but seems to perform better in the study area. The Saastamoinen model assumes that the water vapour pressure decreases with height in a similar manner as the total pressure as:

$$e = e_s \left(T/T_s\right)^{4g/R_d\alpha} \quad [42]$$

Similar to Saastamoinen assumption, the Askne and Nordius model uses:

$$e = e_s \left(p/p_s\right)^{(\lambda+1)} \text{ or } \quad p = p_s \left(T/T_s\right)^{g/\alpha R_d} \quad [43]$$

Equation (14) and equations (32 and 33 combined) according to Askne and Nordius (1987) can be made numerically identical when $\alpha = 6.2\,\mathrm{K/km}$ and $\lambda = 3$. Besides, α and λ are assigned constant values in the Saastamoinen model while variable in the Askne and Nordius model to meet the prevailing environs. Therefore, models, where α and λ can be varied to suit the prevailing environs, produces better accuracy (Askne and Nordius, 1987; Li *et al.*, 2008). Moreover, the numerical values for the refractivity constants k_1, k_2, k_3 used by the Saastamoinen model differ slightly from those used by the Askne and Nordius model. These slight differences in refractivities also contribute to the varying performances of the models in the study area. The Marini and Murray and Niell models performed comparably to that of the Saastamoinen model since they both stem from the Saastamoinen model. Hopfield model, on the other hand, assumes that the wet refractivity decreases with height above the earth surface in about the same manner as the dry refractivity where $g/R_d\alpha - 1 = 4$ with g = 980cms^{-2} and α = 6.828°C/km. This assumption according to Hopfield (1969) corresponds in regions of the earth where this lapse rate value is a realistic value in the troposphere. However, this assumption may differ from reality since g and α obviously vary with latitude and/or season respectively (Li *et al.*, 2008) and this contributed to the poor performance of the Hopfield model in the study area. The use of lengths of position vectors instead of heights by the Goad and Goodman model might contribute to its performance over the Hopfield model. Of all the models evaluated, the Black model performed better in estimating the ZTD in the study area followed by the Askne and Nordius model which did not differ much from the Black model. Saastamoinen, Marini and Murray, Niell, Goads and Goodman, and Hopfield models respectively performed poorly. The performance

of Black and Askne and Nordius models are in agreement with (Chen *et al.*, 2014) and (Li *et al.*, 2008).

Furthermore, the result from the multiple comparison test as shown in Figure 4 and Table 4 indicates that the mean of group 1 (i.e. AN) in blue is considered to be significantly different from group 3, 4, 5, 6 and 7 (i.e. GG, HOP, MM, NIELL and SAAS) in red and with small p-values (0.000) at 95% confidence level, but not significantly different from group 2 (Black) shown in grey and with p-value > 0. Thus, the performance of Black and AN are significantly different from that of GG, HOP, MM, NIELL and SAAS models at 95% confidence level in the study area.

4.2. Models assessment based on the positional accuracies

To further analyse the performance of the prediction models and their impact on positional accuracies, the baseline coordinate solutions from each prediction model were analysed. The results in Figure 6, 7 and 8 indicate that ignoring the application of tropospheric model (strategy I) leads to unreliable baselined results with large bias and RMS errors compared to strategy II (application of tropospheric models). The results also did not show much significant variation in the coordinate difference provided by the application of the prediction models. However, the Black and Askne and Nordius models continue to show superior performance over the other models. It can also be seen from Figure 6, 7 and 9 that positional impact of the tropospheric delay in the horizontal component is more on the North than the East. This is in agreement with the study conducted by Odumosu *et al.* (2015). It can further be observed that the longer the baseline the more the impact of the tropospheric delay resulting in large biases or residuals. This affirms the assertion that tropospheric delay is a distant-dependent error (Yahya and Kamarudin, 2005; Dodo *et al.*, 2019). The results further revealed in Figure 10 that the error in the height component increases with increasing baseline height difference (ΔH).

5. Conclusion

The accuracy of tropospheric delay prediction models plays a critical role in precise GNSS positioning applications. This paper evaluated and analysed the performances of seven tropospheric delay models for modelling and mitigating tropospheric delays using six selected CORS over four regions of Ghana. Firstly, the models were evaluated based on the estimated ZTD using the 1˚ gridded VMF3 ZTD product as a reference. The analysis showed that the Black model performed better followed by Askne and Nordius model. Saastamoinen, Marini and Murray, Niell, Goad and Goodman, and Hopfield models performed poorly in the order given. The MCT performed on the RMSE of the models ZTD revealed that the Black and Askne and Nordius models produced results that are significantly different from the other models at a 5% significance level in the study area.

To further investigate the impact of the tropospheric delay models on positional accuracies, the baseline coordinates solutions from each prediction model were also analysed using corresponding

coordinates solutions from the CSRS-PPP online positioning service as a reference. The results showed that:

I. Neglecting the application of a tropospheric delay model in the baseline processing leads to unreliable baseline results.

II. There was not much variation in the coordinate difference provided by using the prediction models. However, the Black and Askne and Nordius models remained dominated over the other models.

III. Positional impact of the tropospheric delay in the horizontal component is more on the North than the East.

IV. Increase in the baseline length increases the impact of the tropospheric delay leading to large biases or residuals.

V. The residuals in the height component increase with increasing baseline height difference.

Based on the results, either Black or Askne and Nordius model is recommended for estimating and mitigating tropospheric delay in the study area for positioning and navigational applications, however, the choice of Black model will be optimal.

6. Acknowledgements

The authors would like to thank Dr.-Ing Yaw Poku-Gyamfi from the office of the Licensed Surveyors Association of Ghana (LISAG) for providing the CORS data used in this study.

References

Amir, S. and Musa, T. A. (2011) 'GPS meteorology activities in the Malaysian Peninsula', in *Proc. 10th Int. Symp. Exhibit. Geoinf.(ISG) ISPRS Commission*.

Askne, J. and Nordius, H. (1987) 'Estimation of tropospheric delay for microwaves from surface weather data', *Radio Science*. Wiley Online Library, 22(3), pp. 379–386.

Bevis, M., Businger, S., Chiswell, S., Herring, T. A., Anthes, R. A., Rocken, C. and Ware, R. H. (1994) 'GPS meteorology: Mapping zenith wet delays onto precipitable water', *Journal of applied meteorology*, 33(3), pp. 379–386.

Bevis, M., Businger, S., Herring, T. A., Rocken, C., Anthes, R. A. and Ware, R. H. (1992) 'GPS meteorology: Remote sensing of atmospheric water vapor using the Global Positioning System', *Journal of Geophysical Research: Atmospheres*. Wiley Online Library, 97(D14), pp. 15787–15801.

Black, H. D. (1978) 'An easily implemented algorithm for the tropospheric range correction', *Journal of Geophysical Research: Solid Earth*. Wiley Online Library, 83(B4), pp. 1825–1828.

Black, H. D. and Eisner, A. (1984) 'Correcting satellite Doppler data for tropospheric effects', *Journal of Geophysical Research: Atmospheres*. Wiley Online Library, 89(D2), pp. 2616–2626.

Böhm, J., Möller, G., Schindelegger, M., Pain, G. and Weber, R. (2015) 'Development of an improved empirical model for slant delays in the troposphere (GPT2w)', *GPS solutions*. Springer, 19(3), pp. 433–441.

Chen, B. and Liu, Z. (2016) 'A comprehensive evaluation and analysis of the performance of multiple tropospheric models in China region', *IEEE transactions on geoscience and remote sensing*. IEEE, 54(2), pp. 663–678. doi: 10.1109/TGRS.2015.2456099.

Chen, R. Q., Liu, Y. and Li, X. H. (2014) 'Analysis of tropospheric correction models in navigation satellite system', in *Applied Mechanics and Materials*, pp. 2553–2560.

Dodo, J. D., Ekeanyanwu, U. O. and Ono, M. N. (2019) 'Evaluation of Five Tropospheric Delay Models on Global Navigation Satellite System Measurements in Southern Nigeria', *Journal of Geosciences*, 7(4), pp. 201–211.

El-Rabbany, A. (2002) *Introduction to GPS: the global positioning system*. First Edit. Artech house.

Farah, A. (2020) 'Assessment of BeiDou's Tropospheric Model (IGGtrop) for tropospheric delay correction in northern hemisphere', *Journal of Applied Geodesy*. De Gruyter, 14(1), pp. 29–38. doi: 10.1515/jag-2019-0015.

Goad, C. C. and Goodman, L. (1974) 'A modified Hopfield tropospheric refraction correction model', in *Paper presented at the Fall Annual Meeting American Geophysical Union, San Francisco, California, USA, December 12-17*, p. 28.

Herrera, A. M., Suhandri, H. F., Realini, E., Reguzzoni, M. and de Lacy, M. C. (2016) 'goGPS: open-source MATLAB software', *GPS solutions*. Springer, 20(3), pp. 595–603. doi: 10.1007/s10291-015-0469-x.

Hofmann-Wellenhof, B., Lichtenegger, H. and Wasle, E. (2008) *GNSS — Global Navigation Satellite Systems GPS, GLONASS, Galileo, and more*. doi: 10.1007/978-3-211-73017-1.

Hopfield, H. S. (1969) 'Two-quartic tropospheric refractivity profile for correcting satellite data', *Journal of Geophysical research*. Wiley Online Library, 74(18), pp. 4487–4499. doi: 10.1029/JC074i018p04487.

Hu, Y. and Yao, Y. (2019) 'A new method for vertical stratification of zenith tropospheric delay', *Advances in Space Research*. Elsevier, 63(9), pp. 2857–2866. doi: https://doi.org/10.1016/j.asr.2018.10.035.

Isioye, O. A., Combrinck, L. and Botai, J. (2015) 'Performance evaluation of Blind Tropospheric delay correction models over Africa', *South African Journal of Geomatics*. CONSAS, 4(4), pp. 502–525.

Kleijer, F. (2004) *Troposphere Modeling and Filtering for Precise GPS Leveling*, *Netherlands Geodetic Commission*.

Kos, T., Botinčan, M. and Dlesk, A. (2009) 'Mitigating GNSS positioning errors due to atmospheric signal delays', *Journal of Maritime Studies*, 23(2), pp. 495–513.

Landskron, D. and Böhm, J. (2018) 'VMF3/GPT3: refined discrete and empirical troposphere mapping functions', *Journal of Geodesy*. Springer Berlin Heidelberg, 92(4), pp. 349–360. doi: 10.1007/s00190-017-1066-2.

Lee, S. and Lee, D. K. (2018) 'What is the proper way to apply the multiple comparison test?', *Korean journal of anesthesiology*. Korean Society of Anesthesiologists, 71(5), pp. 353–360. doi: 10.4097/kja.d.18.00242.

Li, Z. W., Ding, X. L., Chen, W., Liu, G. X., Shea, Y. K. and Emerson, N. (2008) 'Comparative study of empirical tropospheric models for the Hong Kong region', *Survey Review*. Taylor & Francis, 40(310), pp. 328–341.

Ma, Y., Chen, P., Liu, H. and Ruan, Q. (2019) 'Establishment of Regional Tropospheric Delay Model in Australia', in *China Satellite Navigation Conference*, pp. 152–162. doi: 10.1007/978-981-13-7751-8_16.

Marini, J. W. and Murray Jr, C. W. (1973) 'Correction of laser range tracking data for atmospheric refraction at elevations above 10 degrees', *NASA report X-591-73-351, Goddard Space Flight Center*.

McHugh, M. L. (2011) 'Multiple comparison analysis testing in ANOVA', *Biochemia medica: Biochemia medica*. Medicinska naklada, 21(3), pp. 203–209. doi: 10.11613/BM.2011.029.

Mendes, V. B. (1999) *Modeling the neutral-atmospheric propagation delay in radiometric space techniques*, *UNB geodesy and geomatics engineering technical report*. Department of Geodesy and Geomatics Engineering Technical Report No. 199, University of New Brunswick, Fredericton, New Brunswick, Canada, 353 pp.

Misra, P. and Enge, P. (2011) 'Global Positioning System: Signals, Measurements, and Performance, revised second ed'. Lincoln, Massachusetts: Ganga-Jumana Press.

Musa, T. A., Lim, S. and Rizos, C. (2005) 'Low Latitude Troposphere: A Preliminary Study Using Gps Cors Data in South East Asia', in *proceedings of ION NTM*, pp. 24–26.

Niell, A. E. (1996) 'Global mapping functions for the atmosphere delay at radio wavelengths', *Journal of Geophysical Research: Solid Earth*. Wiley Online Library, 101(B2), pp. 3227–3246.

Odumosu, J., Ajayi, O., Opaluwa, Y. and Kuta, A. (2015) 'Analysis of the Spatio – Temporal Variability and Impact of Tropospheric Delay on the Positional Accuracy in GNSS PPP Observations', (May 2015), p. 7566.

Opaluwa, Y., Adejare, Q., Suleyman, Z. A. T., Abazu, I. C., Adewale, T. O., Odesanmi, A. O. and Okorocha, V. C. (2013) 'Comparative analysis of five standard dry tropospheric delay models for estimation of dry tropospheric delay in GNSS positioning', *American Journal of Geographic Information*, 2, pp.121–131.

Penna, N., Dodson, A. and Chen, W. (2001) 'Assessment of EGNOS tropospheric correction model', *The Journal of Navigation*. Cambridge University Press, 54(1), pp. 37–55.

Realini, E. and Reguzzoni, M. (2013) 'goGPS: open source software for enhancing the accuracy of low-cost receivers by single-frequency relative kinematic positioning', *Measurement Science and technology*. IOP Publishing, 24(11), p. 115010.

Sanlioglu, I. and Zeybek, M. (2012) 'Investigation On GPS Heighting Accuracy With Use Of Tropospheric Models In Commercial GPS Softwares For Different Heights Investigation On GPS Heighting Accuracy With Use Of Tropospheric Models In Commercial GPS Softwares For Different Heights', *FIG Working Week 2012*, (May 2012), pp. 6–10.

Sanz, J., Juan, J. M. and Hernández-Pajares, M. (2013) 'GNSS data processing, Vol. I: fundamentals and algorithms', *Noordwijk, the Netherlands: ESA Communications, ESTEC TM-23/l*.

Smith, E. K. and Weintraub, S. (1953) 'The constants in the equation for atmospheric refractive index at radio frequencies. in Proceedings of Proc. IRE 41'.

Sun, L., Chen, P., Wei, E. and Li, Q. (2017) 'Global model of zenith tropospheric delay proposed based on EOF analysis', *Advances in Space Research*. COSPAR, 60(1), pp. 187–198. doi: 10.1016/j.asr.2017.03.045.

Sun, Z., Zhang, B. and Yao, Y. (2019) 'A Global Model for Estimating Tropospheric Delay and Weighted Mean Temperature Developed with Atmospheric Reanalysis Data from 1979 to 2017', *Remote Sensing*. Multidisciplinary Digital Publishing Institute, 11(16), p. 1893.

Tuka, A. and El-Mowafy, A. (2013) 'Performance Evaluation of Different Troposphere Delay Models and Mapping Functions', *Measurement*. Elsevier, 46(2), pp. 928–937.

Wang, M. and Li, B. (2016) 'Evaluation of empirical tropospheric models using satellite-tracking tropospheric wet delays with water vapor radiometer at Tongji, China', *Sensors*. Multidisciplinary Digital Publishing Institute, 16(2), p. 186. doi: https://doi.org/10.3390/s16020186.

Xu, G. and Xu, Y. (2016) *GPS: theory, algorithms and applications*. Springer.

Yahya, M. H. and Kamarudin, M. N. (2005) 'The Impact of Tropospheric Delay Towards the Accuracy of GPS', *International Symposium and Exhibition on Geoinformation, Penang, Malaysia*, pp. 5–7.

Yao, Y., Hu, Y., Yu, C., Zhang, B. and Guo, J. (2016) 'An improved global zenith tropospheric delay model GZTD2 considering diurnal variations', *Nonlinear Processes in Geophysics*. Copernicus GmbH, 23(3), pp. 127–136.

Yao, Y., Xu, X. and Hu, Y. (2017) 'Precision Analysis of GGOS Tropospheric Delay Product and Its Application in PPP', *Acta Geodaetica et Cartographica Sinica*, 46(3), pp. 278–287. doi: https://doi.org/10.11947/j.AGCS.2017.20160383.

Yao, Y., Xu, X., Xu, C., Peng, W. and Wan, Y. (2018) 'GGOS tropospheric delay forecast product performance evaluation and its application in real-time PPP', *Journal of Atmospheric and Solar-Terrestrial Physics*. Elsevier Ltd, 175(January), pp. 1–17. doi: 10.1016/j.jastp.2018.05.002.

Younes, S. A.-M. (2016) 'Modeling investigation of wet tropospheric delay error and precipitable water vapor content in Egypt', *The Egyptian Journal of Remote Sensing and Space Science*. Elsevier, 19(2), pp. 333–342. doi: 10.1016/j.ejrs.2016.05.002.

Zhang, H., Yuan, Y., Li, W., Li, Y. and Chai, Y. (2016) 'Assessment of three tropospheric delay models (IGGtrop, EGNOS and UNB3m) based on precise point positioning in the Chinese region', *Sensors*. Multidisciplinary Digital Publishing Institute, 16(1), p. 122.